Polar semiconductor ZnO under inplane tensile strain

Zeyad Alahmed[1,2] and Huaxiang Fu[1]
[1]*Department of Physics, University of Arkansas, Fayetteville, Arkansas 72701, USA*
[2]*Department of Physics and Astronomy, King Saud University, Riyadh 11451, Saudi Arabia*
(Received 2 August 2007; published 31 January 2008)

Zinc oxide under biaxial inplane tensile strains is studied theoretically by first-principles density functional calculations. Different material properties (including structural response of cell shape, chemical bonding, total-energy curvature, electrical polarization, Born effective charge, electronic band dispersion, optical interband transitions, and effective masses) are examined. We found that (1) the c/a ratio decreases in a rather linear fashion with the increasing tensile strain when the inplane lattice constant (denoted as a) of ZnO is varied below a critical transition value of $a_{tr}=1.067a_0$ (a_0 is the equilibrium inplane cell length). However, at $a=a_{tr}$, ZnO exhibits a pronounced structural discontinuity in c/a ratio, as well as in cell volume. (2) The structural discontinuity results from the existence of two energy minima (labeled as A and B), both being metastable. Minimum A is energetically favorable when a is below a_{tr}, while minimum B is more stable when a exceeds a_{tr}. (3) As the inplane lattice constant approaches a_{tr} from below, ZnO becomes markedly soft along the polar c axis, promising a large electromechanical response. (4) At $a=a_{tr}$, spontaneous polarization in ZnO collapses, leading to a polar-nonpolar phase transformation. (5) Despite that the spontaneous polarization vanishes when $a=a_{tr}$, Born effective charge of Zn atom nevertheless increases, demonstrating an interesting anticorrelation. (6) Above a_{tr}, covalent overlapping charge largely disappears between those polar Zn-O bonds collinear with the c axis, indicating that the bonds are predominantly ionic. (7) The polar-nonpolar structural transformation simultaneously gives rise to a direct-indirect band gap transition. When a is above a_{tr}, the valence band maximum is no longer at zone center Γ but at zone-edge H point. Occurrence of indirect band gap originates from the fact that the orbital energy of the top valence state at H shows a sensitive dependence on the inplane strain. (8) At zone center Γ, optical excitations from the top two valence states to the lowest conduction state remain strongly allowed after the structural phase transformation. (9) Accompanying the occurrence of the indirect band gap transition is a considerable reduction of the hole effective mass, and hence a large increase of hole mobility.

DOI: 10.1103/PhysRevB.77.045213 PACS number(s): 71.55.Gs, 71.15.Nc, 64.70.K−

I. INTRODUCTION

Zinc oxide of wurtzite structure is a polar solid of growing interest in terms of revealing fundamental knowledge, since it exhibits many unusual properties such as being a wide-gap semiconductor while simultaneously being an efficient piezoelectric of spontaneous polarization. This is witnessed by a considerable amount of work devoted to the ZnO substance; examples are studies of overcoming the doping bottleneck,[1] diffusion of hydrogen impurity,[2] spontaneous polarization and piezoelectricity,[3] stress and temperature dependence of piezoelectric constants,[4] and origin of large electromechanical response in ZnO.[5] The existence of spontaneous polarization in ZnO allows it to couple strongly with external electric fields, which adds to a new degree of freedom to tune physical and/or chemical properties. As a matter of fact, ZnO displays the largest electromechanical d_{33} response among known wurtzite semiconductors, where the d_{33} coefficient characterizes the c axis length change upon application of an electric field along the polar axis (the d_{33} values and other physical quantities of different wurtzite semiconductors are compiled in Table I for comparison[6]).

Technologywise, ZnO is a promising candidate for semiconductor lasers and photodiodes in ultraviolet wavelength with large exciton binding (~60 meV).[7] When doped, ZnO also shows a high electrical conductivity and is thus a good transparent conductor.[8,9] Another interesting technological possibility of utilizing the spontaneous polarization in ZnO is to develop so-called polarization electronics,[10] in which new electronic and/or photonic devices are designed by heterostructuring ZnO with ferroelectric perovskites such that charge density at the interface can be varied as a result of polarization matching. Driven by the fundamental and technological interest, a better understanding of the material properties of ZnO is thus of particular relevance.

Application of inplane strain has been an effective approach for the purpose of modifying cell structure and atom-atom interaction, and subsequently to investigate micro-

TABLE I. Properties of some semiconductors in wurtzite structure, including band gap E_g, lattice constants (a and c), electromechanical d_{33} coefficient, and melting temperature T_m (Ref. 6).

Compound	E_g (eV)	a (Å)	c (Å)	c/a	d_{33} (pC/N)	T_m (°C)
ZnO	3.43	3.249	5.207	1.603	12.4	2300
GaN	3.50	3.160	5.125	1.622	0.73	>1700
AlN	6.20	3.110	4.980	1.601	1.46	3273
ZnS	3.91	3.822	6.260	1.638	3.66	2103
ZnSe	2.87	3.996	6.626	1.658		1793
CdS	2.58	4.135	6.714	1.624	9.71	1750
CdSe	1.83	4.299	7.010	1.631	7.84	1514

scopic knowledge and insight on structure-properties correlation. When applied to semiconductors, modification of cell structure by strain is even more revealing because the band dispersion and optical properties of semiconductors depend critically on the length and angle of chemical bonds. With the advance in molecular beam epitaxy (MBE), the technique becomes far more sophisticated in the sense that strain can be varied in a controllable manner. In ZnO, hybridization exists between Zn $3d$ states and O $2p$ states, which may be altered significantly by imposing inplane strain. Moreover, for polar semiconductor such as ZnO, strain can provide additional knowledge since the lattice length often couples strongly with spontaneous polarization (known as strain-polarization coupling), yielding the interplay among geometric structure, electronic properties, and electrical polarization.

Despite the obvious importance, strain effects in ZnO nevertheless remain not completely understood, particularly for tensile strain in the regime of finite magnitude. In this study, we are primarily interested in tensile strain because many other semiconductors have inplane lattice constants larger than that of ZnO (see Table I). Also, we are interested in studying strains of finite (rather than infinitesimal) magnitude since the effects due to small strain can be investigated more effectively by density functional perturbation theory.[11] In fact, our results of ZnO under finite strains show some interesting properties that do not exist in small-strain regime (see below). Regarding effects of finite strains, relevant reasons that lead us to conduct this computational study are as follows: (i) A *quantitative* determination of how in-plane strain changes the cell volume, internal atomic positions, and chemical bonds in ZnO remains lacking, that is, a study concerning structural properties. (ii) It is of useful value to determine how effective charge and polarization in ZnO may be influenced by inplane strain and in what strain range the polarization continues to remain significant—that is, a property addressing electrical polarization. (iii) One key consequence of applying strain to a crystal is that atomic displacement and cell-shape distortion can affect the band structure of the solid. We are thus naturally led to examine how a finite tensile strain may modify the electronic structure and optical properties in ZnO, which could be needed for various applications. Furthermore, (iv) effects of finite strains on electron and hole masses in ZnO are unknown, which is a problem related to the transport properties of carriers. The purpose of this paper is to obtain a useful understanding of the different properties of technological ZnO under tensile strains and to answer the specific questions described above.

Strain effects in semiconductors depend on the loading direction as a consequence of the fact that the covalent bonding in these substances is highly directional. Since it is preferred in electronic applications that ZnO maintains a crystal symmetry similar to the wurtzite structure (namely, the two inplane lattice vectors are equivalent but differ from the polar c axis) so that the strained ZnO can be conveniently used to form heterostructures with other wurtzite semiconductors, we hence study biaxial inplane strains. Note that the biaxial inplane strain will also alter the c-axis length, allowing us to examine the strain-polarization coupling. Previously, Kulkarni *et al.* investigated the strain-stress relationships and

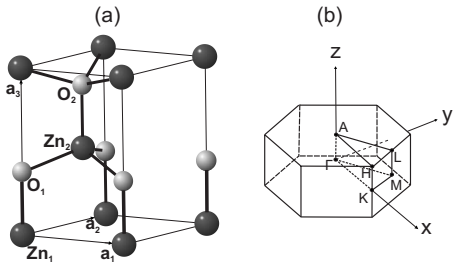

FIG. 1. (a) Primitive cell of wurtzite ZnO crystal, where two Zn atoms are labeled as Zn_1 and Zn_2 and two O atoms as O_1 and O_2. Cartesian x and z axes are along the $\mathbf{a}_1+\mathbf{a}_2$ and $\mathbf{a}_3$ directions, respectively. (b) Brillouin zone of wurtzite crystal.

structural properties in ZnO nanobelts[12] and nanowires[13] under uniaxial tensile loading, mainly using molecular dynamics simulations with interatomic potentials. They observed that the strain-stress relations are significantly different in structures grown along different directions and, in particular, a tensile loading along the growth axis in the $[01\bar{1}0]$ wires was reported to trigger a structure phase transformation.[13] Our work differs from these previous studies in two aspects: (1) The previous studies investigated uniaxial loading while we are interested in biaxial strains. (2) A key outcome of this work is to understand various materials properties—effective charge and polarization, electronic and optical properties, and effective masses. These properties were not addressed in previous investigations.[12,13]

II. THEORETICAL METHODS

The lattice vectors of the unit cell of wurtzite ZnO are defined as $\mathbf{a}_1=a(1/2,\sqrt{3}/2,0)$, $\mathbf{a}_2=a(-1/2,\sqrt{3}/2,0)$, and $\mathbf{a}_3=c(0,0,1)$, where a and c are the inplane and out-of-plane lattice lengths, respectively. Figure 1 shows the primitive cell of the wurtzite structure, containing two Zn and two O atoms. The Zn atoms are located at $\mathbf{r}_1=0$ and $\mathbf{r}_2=(1/3)\mathbf{a}_1+(1/3)\mathbf{a}_2+(1/2)\mathbf{a}_3$, while the oxygen atoms are at $\mathbf{r}_3=u\mathbf{a}_3$ and $\mathbf{r}_4=(1/3)\mathbf{a}_1+(1/3)\mathbf{a}_2+(1/2+u)\mathbf{a}_3$, where the internal u parameter characterizes the distance between the collinear Zn_1 and O_1 atoms along the c axis.

We study biaxial inplane tensile strain, defined as $\eta_1=\eta_2=(a-a_0)/a_0$, where a_0 is the equilibrium inplane lattice constant. Biaxial strains of small or moderate magnitude can be realized in experiments by epitaxially growing ZnO on substrates of different inplane lattice constants. Another possibility of generating biaxial inplane strains is to use free-standing ZnO nanofilms or nanobelts[14] grown with their normal direction along the crystalline [0001] direction. By *compressing* ZnO nanobelts along the normal direction, a tensile strain in the perpendicular plane is produced, and due to the equivalence of the two inplane directions, this inplane tensile strain is biaxial. For each given a lattice constant, we vary the c length and determine the optimal c/a ratio. Every time the cell shape changes, atomic positions are fully relaxed until the Hellmann-Feynman force on each atom is below 0.01 eV/Å.

With optimized structure (including the cell shape and atomic positions) for a given inplane strain, electrical polar-

ization is determined using the modern theory of polarization[15,16] via geometrical Berry phase of valence wave functions, which is implemented into the in-house code. The Born effective charge Z^* is calculated from the derivative of polarization with respect to displacement of atomic position by finite difference as $Z^* = \Delta \mathbf{P} / \Delta \mathbf{r}$.

Technically, we use a mixed-basis pseudopotential method[17] in solving the Kohn-Sham equation within local density approximation (LDA) of the density functional theory.[18] Troullier-Martins type of pseudopotentials[19] is used to account for the effects of core electrons. Semicore Zn $3d$ states are treated as valence electrons for better accuracy. The ionic configuration used to generate Zn pseudopotentials is $3d^{10}4s^{1}4p^{0.1}$, with pseudo/all-electron wave function matching radii $r^{s,p,d}=2.0$, 2.0, and 2.5 bohrs. The ionic configurations for oxygen-pseudopotential generation are $2s^{2}2p^{4}3d^{0}$ for s and p pseudopotentials and $2s^{2}2p^{3}3d^{0.3}$ for d pseudopotential. The wave function radii used for oxygen are $r^{s,p,d}=1.5$, 1.5, and 2.5 bohrs. In fact, the same Zn and O pseudopotentials and the mixed-basis method were used to study the electronic and optical properties of ZnSe based organic-inorganic hybrid materials,[20] the ferroelectric properties of $Pb(ZrTi)O_3$,[17] and the phonon structure in $SrTiO_3$ under finite electric fields,[21] yielding results in good agreement with available experiments or other theoretical calculations. Considering that these materials [ZnSe, $Pb(ZrTi)O_3$, and $SrTiO_3$] have very different characteristic bond lengths, the fact that our pseudopotentials performed well in all circumstances indicates that these potentials are transferable and able to describe ZnO under strains.

A cutoff energy of 884 eV is used in calculations and yields good convergence. With the mixed-basis method and pseudopotentials described above, ZnO under zero-strain equilibrium condition is predicted to have inplane lattice constant of $a_0=3.25$ Å and internal u parameter of 0.378 (compared to experimental values[22] of $a_0=3.253$ Å and $u=0.382$, respectively). Furthermore, the bulk modulus of ZnO is calculated as 165 GPa, in accordance with another theoretical value of 160 GPa in Ref. 23. Regarding the properties relevant to electrical polarization, we found that the Born effective charges of Zn and O in unstrained ZnO are 2.20 and −2.20, compared to the experimental value[6] of 2.10. When the structure is deformed by finite electric fields, our theoretical electromechanical d_{33} coefficient was previously calculated[5] to be 12.84 pC/N, close to the measurement value[6] of 12.4 pC/N. All these results suggest that our theoretical calculations are reasonably reliable.

III. RESULTS AND DISCUSSIONS

A. Strain-induced structural properties and total energies

Figure 2(a) displays the optimized c/a values corresponding to different inplane lattice constants; the numerical results are given in Table II in case that they may be useful for the reader. Under zero inplane strain, the theoretical c/a value is 1.620, compared to the experimental result of 1.603. As the a length is varied below $1.067a_0$ (this inplane lattice constant will be denoted hereafter as a_{tr} for a reason that will become clear below), our results in Fig. 2(a) reveal that the

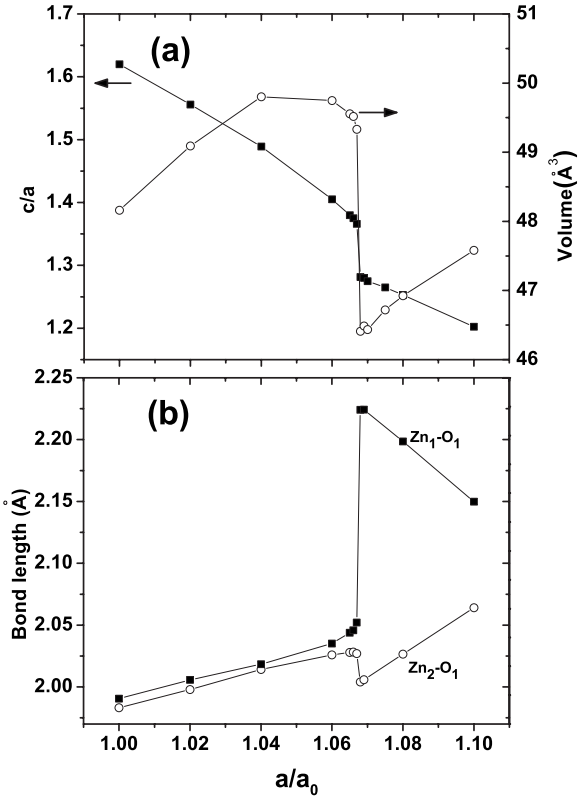

FIG. 2. (a) The c/a ratio (using the left vertical axis) and cell volume (using the right vertical axis) as a function of a/a_0. (b) Lengths of the Zn_1–O_1 bond and the Zn_2–O_1 bond as a function of a/a_0.

TABLE II. LDA-calculated structural parameters of ZnO under different inplane lattice strains. The quantities given in the table include the c/a value, volume (V) of primitive cell, Poisson ratio $-\eta_3/\eta_1$, and c-axis elastic S constant. $a_0=3.25$ Å is the equilibrium inplane lattice length of unstrained ZnO. In the fifth column, S_A and S_B correspond to the elastic constants at minima A and B, respectively (S_B is given in parentheses).

a/a_0	c/a	V (Å^3)	$-\eta_3/\eta_1$	S_A (S_B) (eV)
1.00	1.620	48.16		29.0
1.02	1.556	49.09	1.02	27.8
1.04	1.489	49.80	1.10	22.7
1.06	1.405	49.75	1.35	14.4
1.065	1.380	49.56	1.43	12.3
1.066	1.375	49.52	1.44	11.7
1.067	1.366	49.33	1.50	10.5 (40.2)
1.068	1.282	46.41	2.28	8.4 (36.5)
1.069	1.280	46.49	2.25	(34.3)
1.070	1.275	46.44	2.26	(34.2)
1.075	1.265	46.72	2.14	(34.0)
1.080	1.253	46.93	2.06	(32.7)
1.100	1.203	47.58	1.84	(45.2)

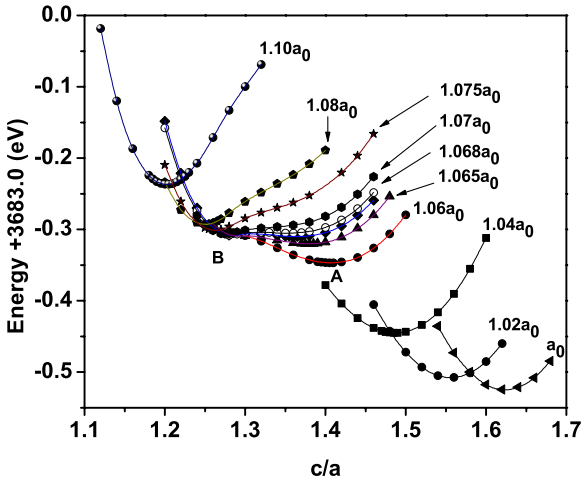

FIG. 3. (Color online) Total energy E versus c/a curves for fixed inplane lattice constant. Each curve corresponds to a different inplane lattice constant whose value is labeled in the neighborhood. The total energy in the vertical axis is given with respect to a base of −3683 eV.

c/a ratio decreases in a nearly linear fashion with the increasing a constant. We numerically found that the c/a curve below a_{tr} can be fairly accurately described by $c/a = -3.955a/a_0 + 5.595$.

However, when the a length is further increased from a_{tr}, an unusual phenomenon occurs. That is, the c/a value apparently undergoes a sudden and discontinuous decline from 1.366 at $a=a_{tr}$ to 1.282 at $a=1.068a_0$ [Fig. 2(a) and Table II], implying the existence of a (first-order) structural phase transition. Interestingly, after the structural transition, the c/a curve recovers its linear behavior but shows a different slope. In fact, fitting the c/a curve for $a>a_{tr}$ now produces $c/a = -2.434a/a_0 + 3.880$. The ZnO solid before and after a_{tr} thus exhibits observable dissimilarity.

To confirm that the unusual c/a discontinuity at a_{tr} in Fig. 2(a) is not an artifact, we further calculate the cell volume under different inplane strain loadings [the empty circles in Fig. 2(a)], showing that the volume expands in the initial stage of small strain and maintains being nearly constant when a/a_0 is between 1.04 and 1.065. Then, at the transition a_{tr} point, the volume declines sharply by more than 6% before it rises again. The structural discontinuity predicted at $a_{tr}=1.067a_0$ is thus real. Our calculations reveal that ZnO under strains should not be assumed to maintain a constant volume, which may otherwise result in error.

We now explain what cause the puzzling structural discontinuity exhibited when ZnO crystal is under tensile strain. Figure 3 depicts the total energy as a function of c/a, each curve corresponding to a fixed inplane a lattice constant. For every data point in Fig. 3, the atomic positions are fully relaxed. When a/a_0 is below 1.04, we see that the E vs c/a curvature is parabolic, with its minimum yielding the optimal c/a that decreases as a is stretched (as expected). However, when a/a_0 is increased to 1.06, the system behaves differently: (1) The energy curve displays not one but two minima (i.e., minima A and B) and both are metastable. (2) The energy near these two minima shows, however, distinctive

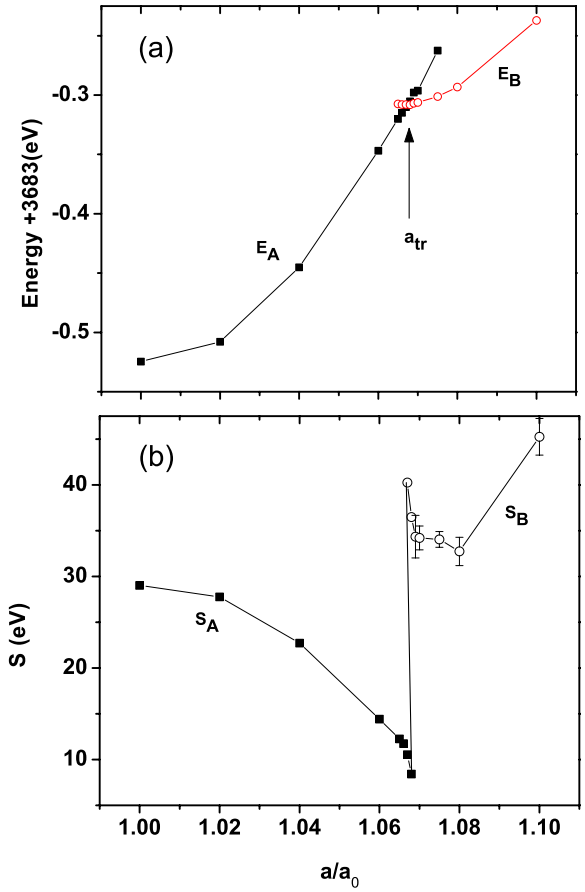

FIG. 4. (Color online) (a) Total energies at minimum A and minimum B as a function of a/a_0. (b) Calculated c-axis elastic S parameter for ZnO under different inplane strains. The total energies in (a) are given with respect to a base of −3683 eV. In (b), the error bars are ±4 eV for S_B immediately above a_{tr} and ±0.5 eV for S_A; these error bars are not drawn in the figure for clarity of display.

parabolicities. More specifically, the curvature near A is flat, whereas the one near B is steep. (3) At $a=1.06a_0$, since minimum A has a lower energy than B, the system thus continues to behave like the one with lower (say, 4%) strains, explaining why the c/a curve in Fig. 2(a) does not show anomalous behavior at $a/a_0=1.06$.

Further increase of the inplane a lattice length leads to a faster rise of the energy for minimum A than for B. More quantitatively, evolutions of the energies for the two minima as a varies are depicted in Fig. 4(a), revealing that the lowest-energy structure switches from A to B at a_{tr}. This gives rise to the observed discontinuity in structural transition. We also note from the total-energy curves in Fig. 3 that, though the optimal c/a ratio for minimum A shifts to lower value as a increases, minimum A does not merge with minimum B. Instead, it disappears when a is sufficiently large.

Fitting of the computed total energies near each minimum to the analytic expression $E=E_{min}+S(c/c_{min}-1)^2$ (where E_{min} and c_{min} are, respectively, the energy value and optimal c-axis length of individual minima in Fig. 3) yields quantitatively the S value associated with the c-axis elastic constant for fixed inplane lattice length. The obtained results are given in Fig. 4(b). From the total-energy curves in Fig. 3, one sees

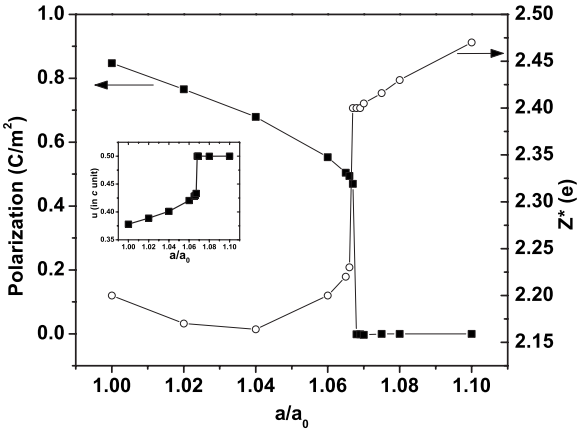

FIG. 5. Polarization (using the left vertical axis) and effective charge Z^*_{33} of the Zn_1 atom (using the right axis) in ZnO of different inplane lattice constants. The internal u parameter, which is the ratio of the Zn_1–O_1 bond length and the c-axis length, is shown in the inset.

obvious difference in terms of curvature near the global energy minimum—between unstrained ZnO and one at $a=1.10a_0$, showing that the c axis is considerably difficult to deform when $a=1.10a_0$. This is hardly surprising since tensile strain shrinks the c-axis length and generally makes it hard to further distort. However, what is interesting is the behavior of the S quantity in between $a=a_0$ and $a=1.10a_0$. Figure 4(b) reveals that when ZnO is in structural A phase, the S constant declines appreciably by nearly 300% before the phase transition occurs. The solid thus becomes markedly soft. The softening of the lattice *along the direction of polarization* can be technologically very useful, since application of a small external electric **E** field collinear with the polar axis will enlarge the **P** polarization—and because of polarization-strain coupling, the enlarged **P** will subsequently lead to the increase of mechanical strain (that is, a process that converts electric energy into mechanical energy). The softer the crystal lattice, the larger the electromechanical response.[24] Our study thus suggests that ZnO, when strained to near $a=1.06a_0$, might drastically enhance its electromechanical efficiency. Meanwhile, we find that the elastic constant along the inplane direction does not change significantly when a is varied below a_{tr}, and the E_A total-energy curve in Fig. 4(a) can be described well as a parabola with curvature of 47.6 eV. As a consequence of the drastically declining elastic stiffness along the polar c axis, the bulk modulus of ZnO will substantially decrease when the material approaches the structure transformation from small strains, since the bulk modulus is simply a linear combination of elastic constants of different components. Finally, Fig. 4(b) further tells us that after the critical a_{tr} point of phase transition, the elastic S parameter undergoes an abrupt increase, transforming ZnO into a much harder solid along the c axis.

B. Strain effects on polarization and effective charge

Figure 5 describes the spontaneous polarization in ZnO under different inplane strains.[25] When $a<a_{tr}$ the polarization declines appreciably as a result of the strain-induced shortening of the c axis, consistent with the theory of polarization-strain coupling. Though declining, the polarization before the structural discontinuity nevertheless remains finite and nonvanishing. This finite magnitude of polarization turns out to be no longer maintained when one continues to increase the tensile strain above a_{tr}. In fact, Fig. 5 reveals that as $a>a_{tr}$, the polarization completely drops to zero, with absolutely no residual magnitude. According to the theory of phase transition,[26] if a quantity is null on one side of the phase boundary and becomes nonzero on the other side of the boundary, this quantity then acts as an order parameter. Our calculation results in Fig. 5 thus explicitly demonstrate that the foregoing structural transformation is a polar-nonpolar phase transition, with polarization as order parameter. The transition is first order, manifested by a discontinuous (rather than a smooth) change in polarization and in c/a. In a previous study,[27] the polar-nonpolar structural transformation in ScN was shown to be a second-order phase transition, without structural discontinuity in c/a ratio. This result in Ref. 27 is not justified by our calculations. On the other hand, our finding of first-order phase transition is consistent with the result in Ref. 13, where the stress-strain relation in $[01\bar{1}0]$ ZnO nanowires under uniaxial tensile strains displays an evident discontinuity at the point of phase transition, though strain loadings are different in our study and in Ref. 13.

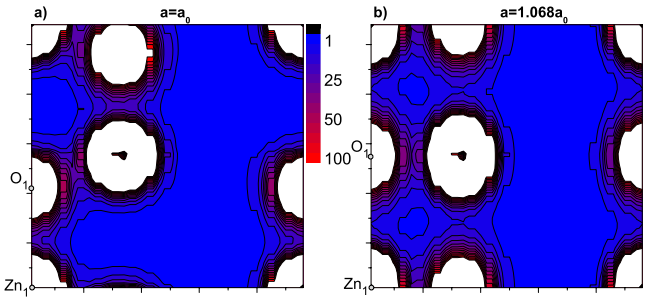

FIG. 6. (Color online) Contour plot of the charge density on the lattice plane that cuts across Zn_1, Zn_2, O_1, and O_2 atoms in Fig. 1(a): (a) For ZnO with $a=a_0$; (b) for ZnO with $a=1.068a_0$. Locations of Zn_1 and O_1 atoms are labeled in the figure; the atom bonded to O_1 from the right is the Zn_2 atom. Charge density near atomic cores is truncated in order to display better the overlapping charge in the interstitial regions between atoms.

The polar-nonpolar phase transition can be more intuitively visualized by examining the electron charge density, shown in Fig. 6. For ZnO in equilibrium, Zn_2 atom (namely, the Zn atom located at half-height of the c axis) and O_1 atom are located at different z planes [Figs. 1(a) and 6(a)]. However, after the structural transition, these two atoms are seated precisely on the same z plane [Fig. 6(b)], leading to a symmetric crystal structure characterized by the existence of a reflection mirror plane that is perpendicular to the c axis and meanwhile passes Zn_2 and O_1 atoms. This is also demonstrated by the internal u parameter shown in the inset of Fig. 5, where, after the phase transformation, u becomes identical to 0.5 (in other words, the O_1 atom is seated at the symmetric midpoint of the $\mathbf{a}_3$ lattice vector). The existence

of the reflection symmetry gives rise to the observed zero polarization. The disappearance of polarization also explains why the c/a curve in Fig. 2(a) displays different slopes before and after the phase transformation, since the c-axis strain couples with polarization in ZnO below a_{tr}, while this polarization-strain coupling no longer exists above a_{tr}.

Next, we study the dynamic Born effective charge Z^* (here, we are interested in the Z^*_{33} component since it is directly related to the c-axis polarization). According to our calculations, the Z^* for two nonequivalent Zn atoms in a ZnO cell are nearly identical for all strain magnitudes considered, so are the Z^* for two O atoms. The sum rule dictates that the Z^* charges of Zn and of O need to be close in magnitude but with opposite signs, which is indeed born out by our numerical values. We thus give in Fig. 5 only the Z^*_{33} value of Zn_1 atom, showing that in polar ZnO phase, when the a length is varied below a_{tr}, the Z^*_{33} changes but very little. However, and interestingly, at the phase transition point, despite the fact that the polarization drops sharply, the effective charge nevertheless *increases*, showing an anticorrelation with the polarization.

The significant increase of the effective charge must indicate a considerable modification of chemical bonding when $a=a_{tr}$, since the Born effective charge is known for being a quantitative measure of how displacement of a given atom in question is influenced by its overlapping interaction with other atoms in the neighborhood.[15] To verify this, we analyze the length of the Zn_1–O_1 bond (to be denoted as d_1 length) and that of the Zn_2–O_1 bond (to be named as d_2 distance). The result is given in Fig. 2(b), revealing that (1) at the a_{tr} transition point, the Zn_2–O_1 bond is nearly intact and the d_2 length varies only by less than 0.03 Å; (2) in contrast, the d_1 length of Zn_1–O_1 bond is enlarged by 0.18 Å at a_{tr}, which is remarkably large and six times of the change of the d_2 length. These results tell us that the chemical bond between Zn_1 and O_1 will break when phase transformation occurs. Indeed, very little overlapping charge density is found between Zn_1 and O_1 atoms, as seen in Fig. 6(b), confirming the existence of a broken bond.

C. Band structure, optical transitions, and effective masses

The computed LDA band structure is given in Fig. 7 for ZnO at $a=a_0$ and at $a=1.068a_0$. For unstrained ZnO (see the upper panel in Fig. 7), the valence band maximum (VBM) at Γ (labeled as Γ_A in the figure) is doublet without counting spin degeneracy; so is the third highest valence state Γ_C. Notably, the second highest valence state, Γ_B, which is singly degenerate, is found to be very close to Γ_A in terms of energy. Analysis of wave functions shows that the broad bands between 0 and −4 eV are mainly from O $2p$ orbitals while the narrow bands between −4 and −6 eV primarily originate from Zn $3d$ orbitals. Zn $4s$ contributes significantly to the lowest conduction band with large dispersion. There are interactions between O $2p$ and Zn $3d$ in various **k** points. The calculated band structure for unstrained ZnO is in overall agreement with those presented in Refs. 3 and 4.

After the phase transition (see the lower panel of Fig. 7), the band dispersion shows two key differences: (1) The single-particle energy of Γ_B is no longer close to Γ_A (unlike in unstrained ZnO); this Γ_B state shifts and becomes close to Γ_C. (2) The H_A electron state at the H point of the Brillouin zone is evidently affected by the inplane strain. In the case of $a=1.068a_0$, the H_A moves up and becomes higher than the Γ_A energy; thereby, the ZnO after critical inplane strain has an indirect band gap. Our calculations thus predict that the polar-nonpolar *structural* phase transformation simultaneously induces a direct-indirect *electronic* band transition.

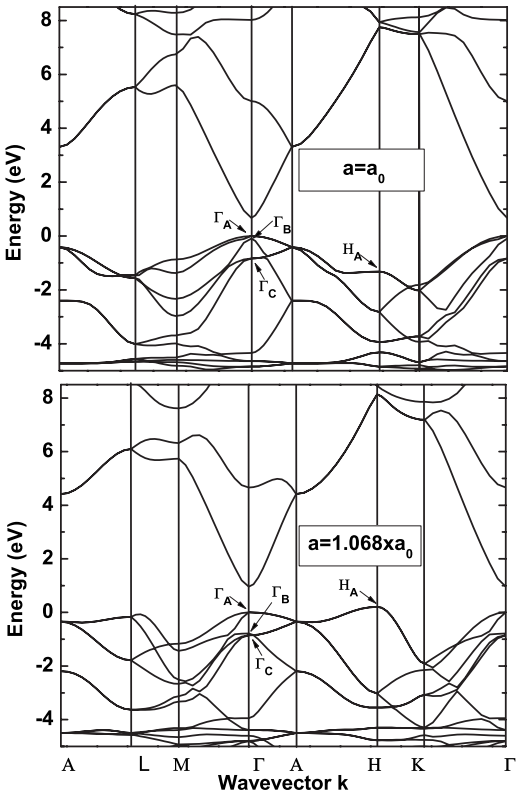

FIG. 7. Theoretical LDA band structure of ZnO at $a=a_0$ (the upper panel) and at $a=1.068a_0$ (the lower panel).

To examine whether the single-particle energies at Γ_B and H_A alter themselves discontinuously at the critical phase transition point or gradually upon the application of inplane strain, Fig. 8 depicts the interband gaps as a function of the inplane lattice constant for direct $\Gamma_A-\Gamma_{CBM}$ and $\Gamma_B-\Gamma_{CBM}$ transitions and for indirect $H_A-\Gamma_{CBM}$ transitions. Owing to the LDA gap problem,[28] as well as the existence of p-d repulsion,[29] our theoretical $\Gamma_A-\Gamma_{CBM}$ gap for unstrained ZnO is underestimated as 0.68 eV, similar to the value of ~0.9 eV obtained in the linearized augmented plane-wave calculations.[3] From Fig. 8, one clearly sees that in addition to the (expected) gradual modification by application of strain, which occurs when $a<a_{tr}$, all gaps are subject to other and discontinuous changes at the phase transition point. More specifically, when ZnO is transformed into nonpolar phase at $a=a_{tr}$, the $\Gamma_B-\Gamma_{CBM}$ gap undergoes the largest discontinuity (by about 0.75 eV) as compared to the other two gaps (~0.25 eV) in Fig. 8. Three transition gaps thus display distinctive behaviors as affected by the phase transition. Figure 8 further reveals that two different factors lead to the formation of an indirect band gap, explaining why H_A becomes the

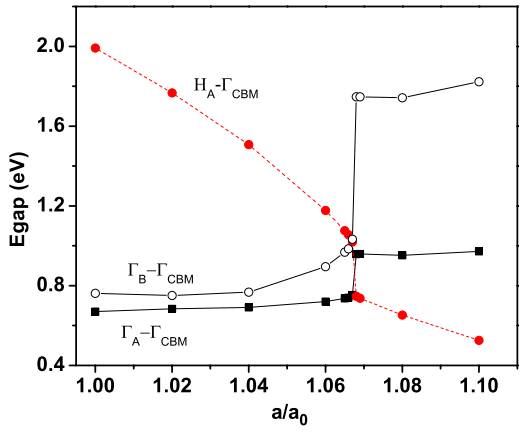

FIG. 8. (Color online) Energy gaps of $\Gamma_A-\Gamma_{\mathrm{CBM}}$, $\Gamma_B-\Gamma_{\mathrm{CBM}}$, and $H_A-\Gamma_{\mathrm{CBM}}$ transitions as a function of a/a_0.

VBM when $a>a_{\mathrm{tr}}$. First, the polar-nonpolar transformation, which changes coordination and chemical bonding, decreases the $H_A-\Gamma_{\mathrm{CBM}}$ gap by 0.3 eV. However, this is not the main factor. The more important factor is the sensitive dependence of the $H_A-\Gamma_{\mathrm{CBM}}$ energy on the gradual evolution of inplane strain. Notably, when the inplane lattice length is varied below a_{tr}, the $H_A-\Gamma_{\mathrm{CBM}}$ gap is altered by the inplane strain in a rather remarkable manner, dropping by nearly 1 eV from a_0 to a_{tr} (Fig. 8). In contrast, the $\Gamma_A-\Gamma_{\mathrm{CBM}}$ gap is least modified, varying quantitatively by less than 0.1 eV when $a<a_{\mathrm{tr}}$, indicating that strain and atomic-position relaxation have little effect on the direct VBM to conduction band minimum (CBM) transition gap at Γ before the phase transition.

It is useful to find how Γ_B and H_A states look like in terms of electron wave functions and why they are substantially influenced by strain and structure phase transition. For this, we plot in Fig. 9 the wave function squares of these two states, for ZnO at a_0 and at $1.068a_0$. By examining atomic components of wave functions (which are naturally included in our mixed-basis method), the Γ_B state in unstrained ZnO is found to result mainly from the O p_z orbitals which have a substantial mixing with Zn d_{3z^2-1}. However, at $1.068a_0$, the Zn d_{3z^2-1} contribution virtually disappears, as seen in Fig. 9, which explains why the energy of this state is affected. Similarly, for H_A state, in unstrained ZnO, it originates from the coupling between Zn $p_z+d_{3z^2-1}$ and O p_z. The superposition of Zn p_z and Zn d_{3z^2-1} makes the wave function near Zn_2 atom nonsymmetric (see the H_A state of unstrained ZnO in Fig. 9). Interestingly, after the phase transition, Zn p_z no longer participates while only Zn d_{3z^2-1} remains, leading to a symmetric wave function distribution around the Zn_2 atom in ZnO of $a=1.068a_0$.

We should point out that our calculations are performed within the local density approximation that underestimates band gap and misplaces the Zn $3d$ bands. Ideally, accurate descriptions of total energy and band structure in ZnO should take into account (1) the quasiparticle correction[30] and (2) the self-interaction correction[31] (SIC), which are beyond our current capability. Here, we merely give a qualitative estimation on how inclusion of these corrections may affect the conclusions on the structural and direct-indirect band gap transitions. First, let us discuss the quasiparticle correction. Quasiparticle calculations tend to rigidly shift the conduction bands while keeping valence band dispersions nearly unchanged.[30,32] Since the structural phase transition predicted here in ZnO is mainly governed by the total energy and involves only the occupied valence states (which are less affected by the quasiparticle correction), this transition is anticipated to remain. Regarding the direct-indirect band transition in this study, a relevant question is how the *relative* orbital energies of the top valence band at non-Γ and at Γ are

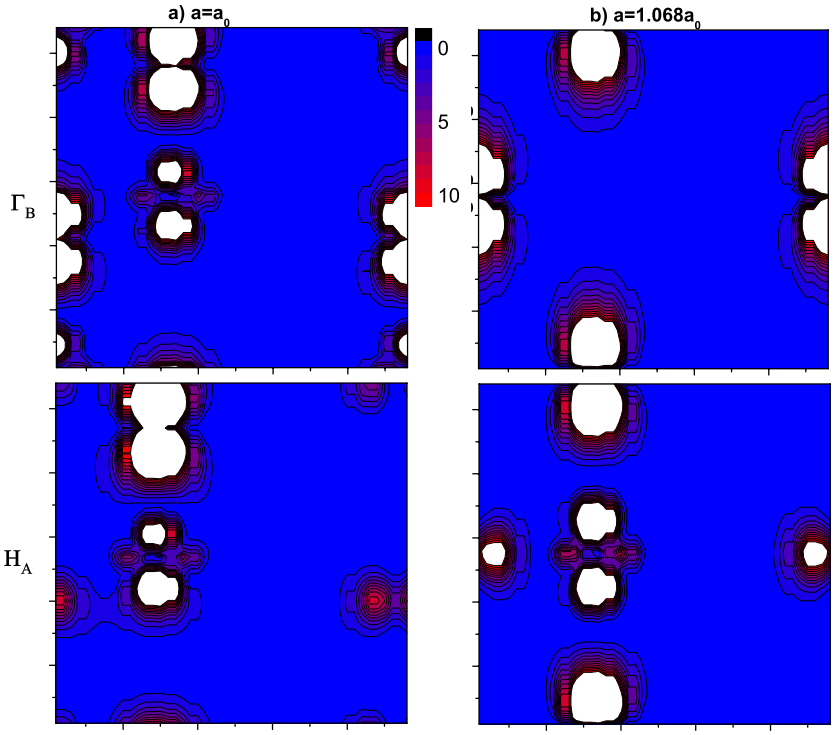

FIG. 9. (Color online) Squared wave functions of the Γ_B state (first row) and the H_A state (second row) at two different inplane lattice constants $a=a_0$ and $a=1.068a_0$. The contour is on the lattice plane that cuts across Zn_1, Zn_2, O_1, and O_2 atoms in Fig. 1(a). For clarity of display, the contours near atomic cores are truncated.

to be altered by the quasiparticle correction. In ZnSe, the energy difference between M_{4v} and Γ_{5v} is 0.81 eV using LDA, and after quasiparticle correction, this difference is barely changed to 0.88 eV.[32] A similar order of modification ($\sim$0.07 eV) was also found[32] in ZnS and ZnTe. In our calculations for ZnO at $a=1.068a_0$ (namely, the strained ZnO immediately after the direct-indirect gap transition), the H_A state is higher than the Γ_A state by more than 0.2 eV (Fig. 8), which is beyond the uncertainty due to quasiparticle correction. Furthermore, as the a length is increased to $1.10a_0$, the orbital energy of the H_A state becomes even higher (by $\sim$0.4 eV) as compared to that of the Γ_A state. We thus think that the direct-indirect band gap transition may still occur after the quasiparticle correction is included. Next, we examine the effects of self-interaction correction. Here, the situation is slightly complex since the shift of Zn $3d$ bands in general changes the dispersion of valence bands. In Ref. 33, the ZnO band structure was calculated using self-interaction corrected pseudopotentials. It was shown that the SIC affects significantly the dispersions of those valence bands *near* the Zn $3d$ bands, in addition to the band gap widening. On the other hand, the band dispersion of the *top* valence band subjects to much less modification. More specifically, the energy difference between Γ_A and H_A states changes from 1.29 to 1.34 eV after the inclusion of self-interaction correction. In view of this rather small modification, our prediction of the existence of the direct-indirect band gap transition is likely to remain even after the SIC is included. Finally, we expect that the polar-nonpolar structure phase transition may not be significantly affected either, since this transition results from the competition of the relative total energies between two rather similar structures (minima A and B). While the SIC may introduce a substantial modification to the absolute total energy, its effect on the relative energy of two *similar* structural phases will be much less. Indeed, the LDA calculations (without SIC) were previously shown to predict well the transition pressure for ZnO to transform from wurtzite to rocksalt structures,[34] even though the wurtzite and rocksalt structures are fairly different.

We now turn to study how the predicted structural transformation may modify interband transitions of optical properties. Since indirect optical transitions require the assistance of phonon and generally have a small probability of occurrence, we will thus focus our attention on direct transitions at the zone-center Γ point. More specifically, we calculate the transition matrix elements, $T_\alpha=|\langle\Psi_v|\hat{P}_\alpha|\Psi_c\rangle|$, caused by light polarized along the α direction. It should be mentioned that one of the important quantities to examine optical properties is the polarization direction of optical absorption or emission (in addition to transition intensity) because one can make use of this polarity to characterize the intrinsic nature of electron states. We find for unstrained ZnO that the doubly degenerate $\Gamma_A\rightarrow\Gamma_{\mathrm{CBM}}$ transitions are strongly allowed, one polarized along x and another along the y direction (in both cases, $T=0.451$/bohr). $\Gamma_B\rightarrow\Gamma_{\mathrm{CBM}}$ is also allowed but polarized along the z axis ($T_z=0.466$/bohr). Calculation results for ZnO at $1.068a_0$ show that after the polar-nonpolar transition, both $\Gamma_A\rightarrow\Gamma_{\mathrm{CBM}}$ and $\Gamma_B\rightarrow\Gamma_{\mathrm{CBM}}$ remain allowed and are, in fact, slightly enhanced. The transition matrix element of the $\Gamma_A\rightarrow\Gamma_{\mathrm{CBM}}$ is increased to 0.482/bohr, while that of the $\Gamma_B\rightarrow\Gamma_{\mathrm{CBM}}$ is enlarged to 0.562/bohr. Different from Γ_A and Γ_B states, Γ_C is found to be optically forbidden to the Γ_{CBM} state and is not affected by the existence of phase transformation. Based on the findings that the $\Gamma_B\rightarrow\Gamma_{\mathrm{CBM}}$ is transition allowed and that the energy of this transition is substantially shifted by the inplane strain, it might thus be possible to monitor the polar-nonpolar transformation using optical spectroscopy.

TABLE III. Effective masses of electron (m_e^*) and hole (m_h^*) as a function of a/a_0. For hole mass, since the VBM is located at H after the structural phase transition, the hole mass at H point is also given. Effective masses in general depend on the direction of band dispersion; two directions (Γ-M and Γ-A) are considered for m_e^* and m_h^* at Γ. The m^* values are in units of the mass of free electron.

	m_h^*				m_e^*	
a/a_0	Γ-M	Γ-A	H-A	H-K	Γ-M	Γ-A
1.000	2.47	2.67	10.01	0.80	0.13	0.13
1.040	2.14	3.13	7.11	0.67	0.12	0.13
1.060	1.99	3.63	5.34	0.59	0.12	0.15
1.069	1.64	6.24	2.73	0.46	0.14	0.20
1.080	1.81	6.53	2.12	0.47	0.14	0.19
1.100	2.09	7.71	2.33	0.47	0.15	0.19

Finally, we determine the electron and hole masses in ZnO under different inplane strains; the results are listed in Table III. The electron masses turn out to be small (around 0.15) for all considered magnitudes of strain, indicating that the electron mobility in ZnO will remain high regardless of inplane strain. For holes, when inplane lattice constant is below a_{tr} (in which the VBM is at Γ), the mass is large and around 2.0 in the Γ-M direction. However, after the crystal is transformed into nonpolar, the VBM is located at H and the hole mass is markedly reduced to only 0.5 along the H-K direction, which is expected to give rise to a drastic increase in the mobility of the hole.

We recognize that the strain magnitude (6.7%) for the structural phase transition to occur is rather large and shall be realized by using external stress loading; growth of ZnO on substrates of this magnitude of lattice mismatch by means of MBE may produce dislocation. One possibility of experimentally examining the predicted structure transition is to use ZnO nanobelts with normal direction along the [0001] crystallographic axis. The nanobelts can be further made into nanomesas by electron beam lithography such that the nanomesas have finite size (on the order of 10–100 nm) along the two directions perpendicular to the [0001] axis. A large inplane strain may be realized by slowly compressing the nanomesas along the [0001] normal direction due to the facts that (1) the slow process allows stress to be effectively relaxed and (2) the finite lateral size can largely prevent the formation of dislocation. As long as the dimension of the nanomesas is not extremely small (otherwise, the structure may be different from wurtzite), the predicted structural phase transition will be observed. Similarly, a large strain may be achieved in short length ZnO [0001] nanocylinders.

By compressing the nanocylinders along the longitudinal direction, a tensile strain will be generated along the lateral directions, and the finite size of nanocylinders along the lateral directions can hinder the occurrence of dislocation. We should also mention that even if all experiments (that other scientists may devise in addition to the two suggested above) turn out to be unable to reach the desirable large strain, our theoretical results presented here are still useful by demonstrating the trends of various properties as well as the underlying physics as the inplane strain is increased. In fact, the characteristic variations in the small and moderate strain regions—including (1) the increase of cell volume, (2) the stretching of both Zn_1–O_1 and Zn_2–O_1 bonds, (3) the softening of the c-axis elasticity, (4) the declining polarization, (5) the substantial increase of the u parameter, (6) the drastic upshift of the orbital energy at H_A with respect to the energy at Γ_A—are all nontrivial and can be verified in experiments.

IV. CONCLUSIONS

A first-principles density functional study has been conducted to investigate the effects of biaxial inplane strain on technologically important polar ZnO semiconductor. Different properties—such as structural response, chemical bonding, electrical polarization, electronic band dispersion, optical transitions, and band-edge effective masses—are examined. We summarize our main findings in the following.

(i) At $a_{tr}=1.067a_0$, both the c/a ratio and cell volume of ZnO are predicted to undergo an evident discontinuity characteristic of the existence of a first-order structural phase transition. (ii) As the structural transformation occurs, the Zn_1–O_1 bond oriented along the polar c axis is broken, as manifested by the large increase in bond length and by the absence of overlapping charge contour between two atoms. (iii) We revealed that ZnO crystals—before and after the critical inplane a_{tr} lattice constant—are located at two different metastable energy minima. These two minima have dissimilar parabolic curvatures. Transition from one minimum to another causes the structural discontinuity. (iv) When ZnO is in minimum A, the lattice becomes markedly soft along the polar axis as tensile strain increases, which poses to considerably enhance the electromechanical efficiency. (v) The phase transition is rigorously identified to be polar-nonpolar type, with polarization as the order parameter. (vi) Though spontaneous polarization vanishes after the structural transition, the Born effective charge of Zn nevertheless rises, revealing an opposite correlation. (vii) The structural phase transformation simultaneously gives rise to a direct-indirect band gap transition. The origin of this electronic transition is predominantly due to the fact that the top valence state at H is substantially affected by the application of inplane strain prior to the occurrence of the structural transformation. (viii) The optical $\Gamma_A \rightarrow \Gamma_{CBM}$ transition is allowed and polarized in the inplane directions, while the $\Gamma_B \rightarrow \Gamma_{CBM}$ is polarized along the polar c axis. Both transitions are slightly enhanced after the structural phase transformation. On the other hand, $\Gamma_C \rightarrow \Gamma_{CBM}$ is optically forbidden. (ix) The electron mass remains to be small (so the electron mobility will maintain high) in the strain range considered in this study. After ZnO becomes nonpolar, the hole mass at H is found to be four times smaller as compared to that in polar ZnO. The polar-nonpolar structural transformation may thus lead to a considerable increase in the hole mobility.

ACKNOWLEDGMENTS

This work was partially supported by the Office of Naval Research and the Center for Piezoelectrics by Design. We thank Ivan Naumov for helpful discussions.

[1] Y. Yan, J. Li, S.-H. Wei, and M. M. Al-Jassim, Phys. Rev. Lett. **98**, 135506 (2007).
[2] M. G. Wardle, J. P. Goss, and P. R. Briddon, Phys. Rev. Lett. **96**, 205504 (2006).
[3] A. Dal Corso, M. Posternak, R. Resta, and A. Baldereschi, Phys. Rev. B **50**, 10715 (1994).
[4] N. A. Hill and U. Waghmare, Phys. Rev. B **62**, 8802 (2000).
[5] D. Karanth and H. Fu, Phys. Rev. B **72**, 064116 (2005).
[6] K.-H. Hellwege and O. Madelung, *Numerical Data and Functional Relationships in Science and Technology*, Landolt-Börnstein, New Series, Group III, Vol. 17a (Springer, New York, 1982); Vol. 22a (Springer, New York,1982).
[7] P. X. Gao, Y. Ding, W. Mai, W. L. Hughes, C. Lao, and Z. L. Wang, Science **309**, 1700 (2005).
[8] F. A. Ponce and D. P. Bour, Nature (London) **386**, 351 (1997).
[9] H. Hayashi, A. Ishizaka, M. Haemori, and H. Koinuma, Appl. Phys. Lett. **82**, 1365 (2003).
[10] T. H. Myers and D. Lederman, MELECON 2006, 2006 IEEE Mediterranean Electrotechnical Conference, 2006 (unpublished), pp. 3–10.
[11] X. Gonze, Phys. Rev. A **52**, 1096 (1995).
[12] A. J. Kulkarni, M. Zhou, and F. J. Ke, Nanotechnology **16**, 2749 (2005).
[13] A. J. Kulkarni, M. Zhou, K. Sarasamak, and S. Limpijumnong, Phys. Rev. Lett. **97**, 105502 (2006).
[14] Z. W. Pan, Z. R. Dai, and Z. L. Wang, Science **291**, 1947 (2001).
[15] R. Resta, Rev. Mod. Phys. **66**, 899 (1994).
[16] R. D. King-Smith and D. Vanderbilt, Phys. Rev. B **47**, 1651 (1993).
[17] H. Fu and O. Gulseren, Phys. Rev. B **66**, 214114 (2002).
[18] W. Kohn and L. J. Sham, Phys. Rev. **140**, A1133 (1965).
[19] N. Troullier and J. L. Martins, Phys. Rev. B **43**, 1993 (1991).
[20] A. Nazzal and H. Fu, Phys. Rev. B **72**, 075202 (2005).
[21] I. I. Naumov and H. Fu, Phys. Rev. B **72**, 012304 (2005).
[22] H. Karzel, W. Potzel, M. Kofferlein, W. Schiessl, M. Steiner, U. Hiller, G. M. Kalvius, D. W. Mitchell, T. P. Das, P. Blaha, K. Schwarz, and M. P. Pasternak, Phys. Rev. B **53**, 11425 (1996).
[23] R. Ahuja, L. Fast, O. Eriksson, J. M. Mills, and B. Johansson, J. Appl. Phys. **83**, 8065 (1998).
[24] H. Fu and L. Bellaiche, Phys. Rev. Lett. **91**, 057601 (2003).

[25] The polarization given here includes the intrinsic pyroelectricity (the magnitude of which is the electron charge multiplied by half of the *c*-axis length).
[26] L. D. Landau and E. M. Lifshitz, *Statistical Physics* (Butterworth-Heinemann, Oxford, 2000), Pt. 1.
[27] V. Ranjan, L. Bellaiche, and E. J. Waller, Phys. Rev. Lett. **90**, 257602 (2003).
[28] L. J. Sham and M. Schluter, Phys. Rev. Lett. **51**, 1888 (1983).
[29] S.-H. Wei and A. Zunger, Phys. Rev. Lett. **59**, 144 (1987).
[30] M. S. Hybertsen and S. G. Louie, Phys. Rev. B **34**, 5390 (1986).
[31] J. P. Perdew and A. Zunger, Phys. Rev. B **23**, 5048 (1981); S. B. Zhang, S.-H. Wei, and A. Zunger, *ibid.* **52**, 13975 (1995).
[32] O. Zakharov, A. Rubio, X. Blase, M. L. Cohen, and S. G. Louie, Phys. Rev. B **50**, 10780 (1994).
[33] D. Vogel, P. Kruger, and J. Pollmann, Phys. Rev. B **52**, R14316 (1995).
[34] S. Limpijumnong and S. Jungthawan, Phys. Rev. B **70**, 054104 (2004).